NASA TM X-53214

JET PENETRATION INTO A LIQUID

by H. G. STRUCK
Aero-Astrodynamics Laboratory

GPO PRICE $ _____

OTS PRICE(S) $ _____

Hard copy (HC) $ _____

Microfiche (MF) _____

TECHNICAL MEMORANDUM X-53214

JET PENETRATION· INTO A LIQUID

By

H. G . Struck

George C. Marshall Space Flight Center

Huntsville, Alabama

ABSTRACT

This investigation is concerned with the phenomenon of a gas jet
impinging on, and penetrating into, a liquid. The study is restricted
to the case of a round jet of subsonic and supersonic velocities pene-
trating the liquid at right angles. The phenomenon was analyzed from
two viewpoints. The first, a stagnation pressure analysis, related the
depth of the surface depression or cavity to the stagnation pressure
based on the centerline velocity of the jet in the neighborhood of the
surface. The second, a displaced liquid analysis which takes the mixing
process of the jet into account, related the weight of the liquid displaced
from the cavity to the momentum of the jet. It was attempted to derive
scaling laws from these investigations to predict penetration depth of
full-scale rocket motors of space vehicles launched from platforms built
over a water surface. Splash heights were also analyzed and correlated.

NASA - GEORGE C. MARSHALL SPACE FLIGHT CENTER

NASA - GEORGE C. MARSHALL SPACE FLIGHT CENTER

Technical Memorandum X-53214

March 8, 1965

JET PENETRATION INTO A LIQUID

By

H. G. Struck

TABLE OF CONTENTS

Page

LIST OF ILLUSTRATIONS

DEFINITION OF SYMBOLS

Symbol	Definition
A	area
d	jet diameter
H	nozzle elevation
n_0	penetration depth
S_c	splash height
S	distance along the drop trajectory
x_c	core length
D	drag force
F	thrust
f	pressure ratio, equations (5) and (6)
M	Mach number
m	mass
P	pressure
q	dynamic pressure
u	velocity of the jet
v	velocity of the gas and liquid drop at the interface
W	weight of displaced liquid
ρ	density
σ	surface tension
γ	ratio of specific heat
γ_L	specific weight of liquid

DEFINITION OF SYMBOLS (Continued)

Symbol	Definition
μ	molecular weight
T^*	total temperature
ψ	slope of cavity

Subscripts

d	liquid drop data
m	jet centerline
o	jet exit
j	jet
∞	condition of the secondary medium or at infinity
i	air water interface, gas data
ch	chamber
w	water

JET PENETRATION INTO A LIQUID

SUMMARY

This investigation is concerned with the phenomenon of a gas jet impinging on, and penetrating into, a liquid. The study is restricted to the case of a round jet of subsonic and supersonic velocities penetrating the liquid at right angles. The phenomenon was analyzed from two viewpoints. The first, a stagnation pressure analysis, related the depth of the surface depression or cavity to the stagnation pressure based on the centerline velocity of the jet in the neighborhood of the surface. The second, a displaced liquid analysis which takes the mixing process of the jet into account, related the weight of the liquid displaced from the cavity to the momentum of the jet. It was attempted to derive scaling laws from these investigations to predict penetration depth of full-scale rocket motors of space vehicles launched from platforms built over a water surface. Splash heights were also analyzed and correlated.

AuTHOR

I. INTRODUCTION

Numerous studies have been made recently on problems concerned with the fluid mechanics of jets in the neighborhood of rigid boundaries. These investigations have been devoted primarily to the determination of velocity and pressure distribution for various configurations. A logical extension of these studies would be the investigation of subsonic and supersonic jets impinging on a deformable surface such as a liquid. Depending on the relative distance of the nozzle above the surface, the gas jet will behave differently due to its structure. While the nozzle position is close to the surface, the potential core plays a major role, and the jet acts like a free streamline jet. For higher elevation, turbulent mixing plays the major role.

The impinging jet causes a depression on the liquid surface which might be shallow in the case of a weak subsonic jet or more like a deep cavity in the case of a strong supersonic jet. Under certain conditions, when the cavities are deep enough, liquid drops are formed and projected from the cavity; the cavity bottom tends to oscillate vertically and the sides laterally. Considerable gas entrainment in the liquid is observed, and surface waves are propagated from the disturbed zone.

II. THE FLUID MECHANICS OF A TURBULENT JET

The simplest case of a jet boundary layer is found during the discharge of fluid with a uniform initial velocity field (u_0 = const.) into a medium moving at constant velocity (u_∞ = const.) or being at rest (submerged jet).

The thickness of the boundary layer in the initial region of the jet starts out with zero at the lip of the nozzle. The thickening of the jet boundary layer, which consists of accelerated particles of the surrounding medium carried along with it and particles of the jet itself that have been slowed down, leads to an increase in the cross section of the jet, as well as to an "eating up" of its nonviscous core. Figure 1 shows a simplified diagram of the jet.

The part of the jet in which there is a core of potential flow is termed the initial region. The static pressure within the jet is assumed to be constant, and as a result of this, the velocity in the potential core remains constant. The centerline velocity beyond the initial region decreases rather rapidly, and the jet widens faster as shown in Figure 1.

We distinguish three regions of the turbulent jet.

a. The initial region where the velocity ratio is constant,

$$\frac{u_m}{u_0} = \text{const},\tag{1}$$

and the dimensionless velocity profiles of the boundary layer in sections normal to the jet are similar.

b. The transitional region, beginning with the drop of the velocity on the axis and the absence of similar velocity profiles, terminates when the disturbances have reached the outer boundary of the jet.

c. The main region again is characterized by a universal velocity profile normal to the axis which is the same for compressible as for incompressible jets. The velocity on the jet centerline decreases for the transitional and main region in general as

$$\frac{u_m}{u_0} = \frac{x_c}{x} \quad \text{for } x \geqq x_c.\tag{2}$$

2

Figure 2 shows a comparison of equation (2) with measurements of Reference 1. The simple law represents the velocity decay fairly well, except in the transitional region where the jet velocity does not follow the discontinuity at the end of the potential core, and at large distances where the velocity seems to approach zero faster. The more exact equations, given in Reference 1, result from the integration of the mass, energy, and momentum conservation laws and are implicit expressions and rather involved, and moreover do not give better results in the transitional region where the jet velocity does not follow the discontinuity at the end of the potential core, and at large distances where the velocity seems to approach zero faster. The more exact equations, given in Reference 1, result from the integration of the mass, energy, and momentum conservation laws and are implicit expressions and rather involved, and moreover do not give better results in the transitional region.

The length of the initial region, sometimes referred to as the length of the potential core x_c, depends on a number of parameters.

a. With increasing Mach number, the core length x_c increases as shown in Figure 3, where the core length for ideally expanded jets is plotted versus the velocity ratio $(u/u_{max})^2$. With the expansion ratio as parameter, one notices that over expanded jets $P_0/P_\infty < 1$ have a shorter core length. Two curves are shown in Figure 3 for the expansion ratio of 1 from different references [1, 2]. The experimental points are scattered between these two curves. The curve of Reference 2 has no theoretical backing and is drawn tentatively according to the experiments with hot and cold jets.

b. With increasing total temperature T_0^* of the jet, the core length x_c decreases, also shown in Figure 3. Chemical reaction, however, is not included. According to Reference 1, it has some effect on the core length, especially when the flame front moves closer to the boundary of the potential core. The curves for different θ^* in Figure 3 are established with the simplified theory of Reference 1 for heated air jets only with total temperatures higher or lower than the total ambient temperature, T_∞^*. If we want to apply the curves to other gas compositions, we have to take their density into account.

$$\theta^* = \frac{T_0^*}{T_\infty^*} \frac{\mu_\infty}{\mu_0} \left(1 - (\frac{u}{u_{max}})^2 \right) \tag{3}$$

where

$$\left(\frac{u_o}{u_{max}}\right)^2 = M*^2 \left(\frac{\gamma - 1}{\gamma + 1}\right). \tag{4}$$

c. Under- and over-expanded jets, $P_o > P_\infty$ and $P_o < P_\infty$, respectively, have different potential core lengths and completely different structures of the core itself. We encounter a system of expansion and compression waves, and consequently, changes in velocity and density for supersonic jets. The core length increases for an under-expanded jet and decreases for an over-expanded jet as shown in Figure 3.

These are the most important parameters for our jet penetration problems. In Reference 2, some rockets were tested and their core lengths were plotted. No appreciable difference was observed compared with the cold air jets. However, the authors agree that a "hot" jet (rocket jet) has a reduction in core length (a figure of 20 percent was quoted). The reduction in core length of hot air jets is confirmed by experiments carried out by Yakovlevsky and Pechenskin [1, p. 304], and they agree very well with the simplified theory of Reference 1. Compressible jets impinging at a right angle on an obstacle develop a detached shock wave in front of it, provided the centerline Mach number of the jet M_j is greater than 1. The pressure at the stagnation point is then given by the Pitot pressure relation which depends only on the Mach number just in front of the normal shock region on the centerline of the jet.

For the case $M_j \geq 1$, the ratio of the compressible to the incompressible stagnation pressure is given by the Pitot pressure relation

$$\frac{\Delta P}{q} = f = \frac{4}{\gamma + 1} \left(\frac{M_j^2 - 1}{M_j^2}\right) + \frac{\gamma + 1}{\gamma} \left[\frac{(\gamma + 1)^2 M_j^2}{4\gamma M_j^2 - 2(\gamma - 1)}\right]^{\frac{1}{\gamma - 1}} - \frac{4\gamma M_j^2 - 2(\gamma - 1)}{\gamma(\gamma + 1) M_j^2}, \tag{5}$$

which consists of the adiabatic compression due to the shock and the isentropic compression between shock and stagnation point.

4

For $M_j \leq 1$, no shock exists, and the adiabatic compression of the subsonic jet is considered, which is, for this case,

$$\frac{\Delta P}{q} = f = \frac{2}{\gamma M_j^2} \left\{ \left[\frac{\gamma - 1}{2} M_j^2 + 1 \right]^{\frac{\gamma}{\gamma - 1}} - 1 \right\}. \tag{6}$$

Figure 4 shows the pressure ratio versus the jet Mach number for different values of the ratio of specific heat, γ. We notice that for high Mach numbers the curves approach a value of approximately 1.8.

III. THE ANALYTICAL MODELS FOR THE JET PENETRATION

The following is taken from Reference 3 with only minor modifications. Figure 5 explains all dimensions and parameters.

1. The Stagnation Pressure Analysis

We assume that the maximum penetration depth n_o is equal to the dynamic pressure of the jet at the centerline, and the velocity in the liquid is zero.

$$q \cdot f = \frac{1}{2} \rho u_m^2 f = \gamma_L n_o. \tag{7}$$

This equation accounts for the compressibility of the jet. Like u_m, so is f a function of x/d_o for constant specific heat ratio γ. Since the Mach number of the jet centerline M_j can be expressed in terms of u_m/a_{ch} or $(u_m/u_o) M_{ex}$,

$$M_j^2 = \left(\frac{u_m}{a_{ch}} \right)^2 \left(1 - \frac{\gamma - 1}{2} \left(\frac{u_m}{a_{ch}} \right)^2 \right)^{-1} = \frac{\frac{u_m^2}{u_o^2} M_{ex}^2}{\left[1 - \frac{\gamma - 1}{2} M_{ex}^2 \left(\frac{u_m^2}{u_o^2} - 1 \right) \right]}, \tag{8}$$

where a_{ch} is the total speed of sound given by chamber conditions.

The velocity u_m on the centerline is given by equation (2), and the thrust of an ideally expanded jet $P_0/P_\infty = 1$ equals to

$$F = \frac{\pi}{4} \rho d_0^2 u_0^2,$$ (9)

which is the momentum of the jet at the exit and which stays constant. Equations (2) and (9) inserted into equation (7) and with x the distance from the nozzle to the stagnation point replaced by $(H + n_0)$, we obtain a dimensionless expression

$$\frac{F}{\gamma_L u_0 d_0^2} = \frac{\pi}{2f} \left(\frac{1}{x_c/d_0}\right)^2 \left(\frac{H + n_0}{a_0}\right)^2.$$ (10)

When we introduce the velocity law given by equation (2), we assume that the dynamic pressure decay is not affected by the entrainment of water drops. However, this assumption is not necessary for the core, since no water can enter this region.

2. The Displaced Liquid Analysis

The momentum of a jet, which is equal to the thrust of an ideally expanded jet, is conserved and carried over to the liquid which is displaced. We assume now that the component of the momentum of the departing gas in the direction of the jet is small and negligible. Then one can set the thrust equal to the weight of the displaced liquid. It is further assumed that the cavity profile is established by a known pressure distribution obtained from circular jets impinging on a solid surface and that the depression is sufficiently small that the change in shape of the liquid surface does not appreciably alter the velocity and pressure distribution of the gas flow.

The pressure distribution of a submerged circular liquid jet impinging on a flat submerged plate was experimentally obtained by Poreh and Cermak [3]. The static pressure distribution of a gas jet impinging on a flat plate, which is shown in Figure 6, is another experimentally obtained curve [8]. An error curve approximation agrees fairly well with the experimental data of References 3 and 8 for a value of $\beta \approx 130$ (Figure 6). For the general investigation, β must be variable to account for the difference of Mach number, temperature, expansion, ratio, etc., of the jets.

6

$$\frac{n}{n_o} = \exp\left\{-\ \beta(r/H)^2\right\}.$$ (11)

The displaced liquid weight is then given by integrating the volume multiplied by the specific weight of the liquid.

$$W = \gamma_L V = \frac{\gamma_L \pi\ H^2\ n_o}{\beta}.$$ (12)

Instead of the elevation of the nozzle above the flat plate H, we introduce now the elevation of the nozzle above the water level plus the penetration depth n_o, to obtain the same distance of the nozzle from the stagnation point, $n_o + H$. The thrust of the jet shall now be equal to the weight of the displaced liquid according to the previously stated assumption. We obtain

$$\frac{F}{\gamma_L\ n_o\ d_o^2} = \frac{\pi}{\beta}\left(\frac{n_o + H}{d_o}\right)^2.$$ (13)

Equating equations (10) and (13), we find the expression for β as

$$\beta = 2f\left(\frac{x_c}{d_o}\right)^2.$$ (14)

The left side of equation (13) represents a thrust-weight ratio where the volume of the liquid is $n_o d_o^2$. The minimum penetration depth of a jet can be obtained from (13) by replacing F with the right side of equation (9).

$$\frac{\pi}{2f}\left[\frac{\frac{\rho}{2}\ u_m^2 f}{\gamma_L\ n_o}\right]\frac{u_o^2}{u_m^2} = \frac{\pi}{2f}\left(\frac{x_o + H}{x_c}\right)^2.$$ (15)

The term in the square bracket is equal to one according to equation (7), and therefore is $(n_o + H) \geq x_c$; i.e., the nozzle elevation plus penetration depth into the liquid is equal to the core length of the initial region x_c. For this case the stagnation point moved into the transitional region of the jet for which no universal velocity profile exists, and consequently the pressure distribution on a solid surface due to an impinging jet will change with the axial distance. However, we assume that the difference between the velocity profiles of the main and transitional region is of minor consequence as the change in the pressure distribution of a jet impinging on a solid or liquid surface.

By combining all Mach number dependent terms, we can find a "universal" curve which will be the point of departure for the model laws:

$$\frac{n_o + H}{d_o} = \frac{x_c}{d_o} \sqrt{f} \sqrt{\frac{2F}{\gamma_L \pi d_o^2 n_o}} , \qquad (16)$$

where f is the function shown in Figure 4. It depends on the jet Mach number M_j (the Mach number in front of the normal shock), which is, on the other hand, a function of the exit Mach number M_{ex} and the dimensionless standoff distance $(n_o + H)/d_o$ of the nozzle. By setting

$$C_1 = \left(\frac{x_c}{d_o}\right)^2 \left(\frac{2F}{\gamma_L \pi d_o^3}\right), \qquad (17)$$

which is essentially a function of the Mach number for ideally expanded jets, we can express equation (16) as

$$\frac{n_o + H}{d_o} = \frac{\sqrt{C_1 f}}{\sqrt{\frac{n_o}{d_o}}} . \qquad (18)$$

8

The maximum influence of f on the penetration depth $(n_o + H)/d_o$ can be obtained from equation (18) by setting $H = 0$:

$$\left(\frac{n_o}{d_o}\right)^3 = \frac{f}{d_o}\left[\left(\frac{x_c}{d_o}\right)^2 \frac{2F}{\gamma_L \pi d_o^2}\right]. \tag{19}$$

We notice that the penetration increases only with the cubic root of f. The term in the square brackets is constant for an ideally expanded jet of a given Mach number. Equation (19) shows also that for increasing exit diameter the relative penetration (n_o/d_o) decreases. The core length (x_c/d_o) can be obtained from Figure 3 if the jet expands ideally. For over- or under-expanded jets, an equivalent core length must be taken which is also shown in Figure 3. On the other hand, the core length can be obtained from testing a scale model of the prototype.

IV. DISCUSSION OF THE TEST RESULTS

A literature survey showed that already a multitude of tests are available which deal with penetration of gas jets into liquids. Now additional tests were conducted in References 5, 6, 9, and 10, which were correlated with existing data.

In Figure 7 the dimensionless penetration depth n_o/d_o was plotted versus the dimensionless height of the nozzle above the water level. The theoretical curve was obtained from equation (18). A good representation is given for a range of H/d_o between 0 and approximately 30. For higher H/d_o values, the actual penetration is less than the predicted one. This could be partly explained by the insufficient representation of the velocity by the simple equation (2). The jet velocity seems to vanish faster than the hyperbolic velocity law. Figure 8 shows the approximate Mach number M_j on the centerline along the length of the jet. It was obtained by equation (8) using for u_m/u_o the curve of Figure 2 for $M_{ex} \approx 3.0$. The minimum distance between nozzle and stagnation point of the three jets of Figure 7 is $(n_o + H)/d_o \approx 50$. A comparison with Figures 8 and 4 shows that the jet Mach number is in the low subsonic range and the influence of $\sqrt{f}$ on the penetration depth n_o/d_o is approximately 1.03.

Figure 9 shows the data of "cold" air jets for different Mach numbers M_o and different nozzle heights H/d_o. Within the accuracy of the experiments, equation (10) correlates the data fairly well. The flagged symbols indicate test results where $H/d_o = 0$. We observe that the stagnation point

9

is located far downstream in the main region of the jet where the jet Mach number is already subsonic. Apparently, the water entrainment into the boundary layer of the jet has little effect on the assumption that the momentum along the jet is constant as pointed out by the coincidence of experiments and theory. When we enter experimental points of larger $H/d_o > 30$ to 40, the agreement becomes worse, as expected, since Figure 6 shows a departure from experiment and theory. The penetration for $H > 30$ becomes less as theory predicts, and consequently, the point must lie on the left side of the corresponding theoretical curve. This departure is partly due to the adoption of the simplified velocity decay function as given by equation (2).

In Figure 10 "hot" data are plotted for different tests. Again, equation (10) gives a good approximation, as mentioned in the discussion of Figure 2. Since the experiments show some scatter, it is more appropriate to use a band for a certain Mach number instead of a single curve. Furthermore, the jets are not all expanded ideally so that the core length varies too.

Figure 11 shows a "universal" plot where all available data of ideally expanded jets were used. The data are now independent of the Mach number dependent core length for relatively large penetrations n_o/d_o. Equation (16) was used to correlate all available data. However, for small penetrations ($x_c \sim n_o$) and a given Mach number, the curve will branch off to different values of the ordinate which are identical to the core length x_c/d_o as shown by equation (15). Also the influence of the factor f will be important for supersonic jets because the jet Mach number in front of the normal shock is rather high (Figure 8). However, the jet expands now into a region of high pressure which changes the core length to a smaller value. For fully expanded supersonic jets, data of small penetration depth $(n_o + H)/d_o$ are not available. Collecting all available subsonic and supersonic data with their corresponding core length, we obtain Figure 10, where data of References 3 and 7 are plotted. The core length of the subsonic jet is larger, by a factor of 2, than given in Figure 3. This indicates that the jets used for the subsonic impingement test were probably under-expanded. In the literature, concerned with this problem, we find core length varying from 4 to 10 for subsonic jets [3].

In Figure 12, the single-dashed curve now branches off and approaches a value of approximately 8. Data obtained from Reference 3 were in the range from $H/d_o = 4$ to 48, whereas in Reference 7 data for $H/d_o = 0$ were also available. The lowest nozzle elevation of the subsonic test series of Reference 3 was $H/d_o = 4$ with only a negligible n_o/d_o. This could be explained by a shortening of the core of the jet which, positioned closer to the water surface, expands into a region of higher pressure, thus approaching the condition of ideal expansion. Furthermore, the sharp corner of the centerline velocity is not real, as a comparison of the real velocity with the simple law x_c/x in Figure 2 shows.

10

V. MODEL LAWS FOR THE PENETRATION

For the penetration problem, we want to simulate the dimensionless penetration n_o/d_o which shall be the same for prototype and model:

$$\left(\frac{n_o}{d_o}\right)_m = \left(\frac{n_o}{d_o}\right)_p . \tag{20}$$

To achieve this, the expression given by equation (16) must be held constant for model and prototype. Rewriting equation (16) yields

$$\left(\frac{n_o + H}{d_o}\right)^2 \frac{n_o}{d_o} = f \left(\frac{x_c}{d_o}\right)^2 \frac{2F}{\gamma_L \pi d_o^3} . \tag{21}$$

The solution for n_o/d_o is a cubic and can be solved by graphical means. However, for $H/d_o = 0$, we obtain simpler relations which will shed more light on the relationship between the different parameters.

$$\frac{n_o}{d_o} = \left(f \frac{2F(x_c/d_o)^2}{\gamma_L \pi d_o^3} \right)^{1/3} . \tag{22}$$

The penetration depths of model and prototype are equal if the expression on the right side of equation (22) is equal for both model and prototype, respectively.

$$\left(f \frac{F(x_c/d_o)^2}{\gamma_L d_o^3} \right)_m = \left(f \frac{F(x_c/d_o)^2}{\gamma_L d_o^3} \right)_p . \tag{23}$$

Let us first assume that model and prototype have the same pressure differential across the exit plane; i.e., both have the same expansion ratio.

$$P_o/P_\infty = \text{const.} \tag{24}$$

The constant is unity for an ideally expanded jet. For a geometrically scaled model then (the exit Mach number is the same and therefore the thrust per exit area),

$$\frac{F}{\frac{\pi}{4} d_o^2} = \left[\frac{2\gamma}{\gamma - 1} P_{ch} \left(\frac{u}{u_{max}} \right)^2 \left(1 - (\frac{u}{u_{max}})^2 \right)^{\frac{1}{\gamma-1}} \right]$$

$$= \left[\gamma M^2 P_{ch} \left\{ 1 + \frac{\gamma - 1}{2} M^2 \right\}^{\frac{\gamma+1}{2(\gamma-1)}} \right] \tag{25}$$

is identical for both model and prototype, and also the core length x_c/d_o. From equation (23) we obtain for identical γ_L

$$(d_o)_m = (d_o)_p. \tag{26}$$

For this case, the model dimensions are identical with the prototype dimensions, and no scaling is possible.

If we impose no restrictions on the similarity of the model except that of geometric similarity which shall be preserved for model and prototype, then the jet Mach number is the same and with it the factor f and the dimensionless core length (x_c/d_o). Equation (23) becomes now

$$\left(\frac{F}{d_o^2} \frac{1}{\gamma_L} \frac{1}{d_o} \right)_m = \left(\frac{F}{d_o^2} \frac{1}{\gamma d_o} \right)_p. \tag{27}$$

The exit diameter of the model becomes

$$\frac{d_{om}}{d_{op}} = \left(\frac{F}{d_o^2} \right)_m \left(\frac{d_o^2}{F} \right)_p \cdot \frac{(\gamma_L)_p}{(\gamma_L)_m}. \tag{28}$$

12

If the thrust-to-area ratio is not changed and the liquids on which the jets impinge are the same, then we obtain the above-mentioned case again, equation (26). Smaller model diameters are, of course, desired, and therefore the following conditions should be observed:

$$\left(\frac{F}{d_0^2}\right)_m \ll \left(\frac{F}{d_0^2}\right)_p \tag{29}$$

and

$$\left(\gamma_L\right)_p \ll \left(\gamma_L\right)_m. \tag{30}$$

Decreasing $(F/d_0^2)_m$, holding the Mach number of the jet the same as that of the prototype, means decreasing the chamber pressure of the model which can be seen from equation (25). We see that the diameter ratio decreases linearly with the chamber pressure ratio. This, however, means that the experiments have to be conducted in an underpressure chamber to satisfy the condition of pressure constancy at the exit and holding thus the same dimensionless core length.

The second condition states that we have to use a liquid heavier than water, possibly mercury. The reduction in model diameter is then 1/13.5 of the prototype diameter.

More favorable models are obtained when the geometric similarity is abandoned, and subsonic model jets are used to simulate cavities produced by supersonic jets.

Since scaling of geometrically similar models leads to an impractical experimental apparatus, we must abandon this approach. On the other hand, we can readily predict the cavity depth accurately enough, at least within the scatter of the experimental point, by using equations (17) and (18) which we actually used for deriving scaling laws.

VI. SPLASHING

In Reference 3, the investigators observed that splashing occurs after the jet has reached a certain velocity and the penetration depth n_0 is larger than a certain critical depth. An approximate estimate from their results indicates that splashing occurs for a cool air jet impinging normally on a water surface when the centerline velocity u_m is approximately 40 to 50 ft/sec, which corresponds to a critical penetration depth of .04 ft. The Kelvin-Helmholtz interfacial instability relationship [11] predicted an air velocity of about 22 ft/sec. Here, waves on a horizontal surface forming the common boundary of two parallel currents with different velocities u, u' were considered (the dash denotes the velocity of the air). The theory predicts an instability of the waves if

$$|u - u'| > \frac{1 + \frac{\rho'}{\rho_w}}{\sqrt{\frac{\rho'}{\rho_w}}} c_m$$

where ρ_w, ρ' are the densities of water and air, respectively, and c_m the minimum velocity of the waves, which is about .71 ft/sec for an air-water interface. If the relative velocity $|u - u'|$ exceeds this value, which is about 27 ft/sec the amplitudes of the small waves about two-thirds of an inch in length, will continually increase until droplets are formed. The velocity of the water at the surface, when compared to the velocity of the jet, is negligibly small. We can therefore assume that the velocity of the air must exceed this value. We can then form an expression n_0/n_{ocrit} where n_{ocrit} is the penetration depth at which water drops will form for the first time.

Splash heights are a function of the drop velocity v_D at the air water interface (see Figure 5 for explanation of the subscripts). Our goal is now to find a relationship between the splash height S_c and some known parameter of the cavity or the jet. Let us first consider the complete equation of motion for the gas-liquid mixture at the cavity-water interface. We assume a departing gas sheet of constant velocity across the sheet.

The equations which govern the motion of the gas and the liquid drops are the following:

For the gas at the interface, we obtain

$$A_i \rho_i \ ds \ \frac{dv_i}{ds} v_i = - A_i d_p - A_n \ ds \cdot D - \ldots .$$

14

The acceleration of the gas from zero velocity at the stagnation point of the cavity to its maximum velocity at the lip of the cavity is due to the decreasing pressure force $-A_i \, dp$ and the drag of the $A \cdot n \cdot ds$ drops in the gas. Friction forces are neglected. A_i is the area which is occupied by the gas, $A = A_i + A_D$ is the total cross section of the departing mixture and n is the number of water drops per unit volume. To calculate the drag the drop size must be known. An equilibrium drop size can be calculated if the pressure of the surrounding gas, the pressure within the droplet, and the surface tension of the drop are known.

The equation for the liquid drops is

$$A_D \rho_D \; ds \; \frac{dv_D}{ds} \; v_D = - A_D dp + A ds \, nD + (v_i - v_D) \, dm_D - m_D \, A ds \, ng \sin \bar{\psi}.$$

There are several causes of the acceleration of the liquid drops in this element of length ds at a point s: the pressure field acts on the drops, and the gravity and the drag forces which decelerate the drops. Furthermore, new drops formed from the water and vapor may condense onto the drops already formed which might have a lower velocity.

A_D is the area occupied by the liquid and ψ the inclination of the stream-tube to the horizontal. In addition to these equations, the conservation laws of mass, energy, and momentum must be applied plus an equation which determines the formation of drops. This is a very complex problem, and we have to simplify the equation. We consider, therefore, only the trajectory of one drop of constant size.

$$v_i \frac{dv_i}{ds} = - \frac{1}{\rho_i} \frac{dp}{ds} - \cdots$$

and

$$v_D \frac{dv_D}{ds} = - g \sin \psi - \frac{1}{\rho_D} \frac{dp}{ds} + \frac{\rho_i \, c_D \, A_D}{2m_D} \, (v_i - v_D)^2.$$

The velocity of the gas at the interface is given as

$$v_i^2 = u_m^2 \, (s/n_o),$$

where s is counted positive from the stagnation point to the lip of the
cavity. One can express dp/ds now as

$$\frac{dp}{ds} = -\frac{\rho_i}{2}\frac{u_m^2}{n_o},$$

and the combined equations become finally

$$\frac{v_D}{u_m} a\left(\frac{v_D}{u_m}\right) = \left[\frac{\rho_i}{2\rho_D}(1 - \sin\bar{\psi}) + \frac{\rho_L c_D A_D n_o}{2m_D}\left\{\frac{s}{n_o} - 2\sqrt{\frac{s}{n_o}}\left(\frac{v_D}{u_m}\right) + \left(\frac{v_D}{u_m}\right)^2\right\}\right] d\left(\frac{s}{n_o}\right).$$

This differential equation was numerically integrated for different drop
sizes. For large drop sizes small velocity ratios were obtained, and
with decreasing radii the velocity ratio increased until the velocity
ratio became one for vanishing drop sizes. Since all drop sizes are
encountered in the departing gas water mixture, the velocity of the gas
at the lip decreases because of the drag of the water drops. Therefore,
we set $v_D/u_m = 1 - a$, where a is the velocity defect due to the drag of
the n liquid drops. The splash height of a small drop can be approximated
by

$$S_c = \frac{v_D}{2g}\sin^2\psi\, max,$$

where ψ_{max} is the maximum inclination of the droplet trajectory to the
horizontal. For deep cavities, ψ_{max} is of the order of 80°. Small drops
have almost the same acceleration as the gas at the cavity-water inter-
face; therefore,

$$-g\sin\bar{\psi} = v_i\, dv_i/ds$$

$$= u_m^2/2n_o$$

and

$$u_m^2/2n_og \approx \sin\psi.$$

16

Inserting this relation into the above equation for the splash height, we obtain

$$\frac{s_c}{n_o} = (1 - a)^2 \sin^2\psi_{max} \; \sin \bar{\psi}.$$

Figure 13 shows some observed splash heights for penetration 20 to 60 times deeper than the critical depth n_{ocrit}. For small penetration, ratios n_o/n_{ocrit} approaching one $\bar{\psi}$ and ψ_{max} decrease to a small finite value and depend on the cavity diameter-to-depth ratio. For large penetration ratios, the dimensionless splash heights seem to approach $s_c/n_o \approx .7$. These data were obtained from Reference 10. More data, however, are needed to confirm this. Since the cavity oscillates considerably for deep cavities, the splash heights also oscillate at the same frequency. The constant splash in Figure 13 is defined as the minimum height that the splashing water maintains during the test run. On this constant splash height, a distance of twice the amplitude of the oscillation is superimposed to obtain the surging splash. This distance is proportional to twice the amplitude of the cavity oscillation squared.

VII. PENETRATION DEPTH FOR A FULL-SCALE F-1 ENGINE

An example shall illustrate the procedure of calculating the probable penetration depth of a full scale single engine.

The F-1 engine was chosen, with the following data assumed.

Chamber pressure	1000 psia
Exit pressure	6.43 psia (over-expanded)
Exit temperature	2544 °R
Exit Mach number	3.70
Exit velocity	9807 ft/sec
Thrust	1500 K lbs
Expansion ratio	16.0
Exit diameter	11.67 ft = 140 in
Mean specific ratio	1.23.

VIII. THE PENETRATION DEPTH OF AN ENGINE CLUSTER

The preceding discussion dealt with only one engine impinging on a liquid surface. If more engines are added, new additional parameters have to be considered, for instance, the spacing, the geometry of the cluster, and the number of engines. A very important parameter of the single-engine investigation turned out to be the core length. Therefore, it is obvious that the distance between the engines divided by their core length should be held constant. Figure 15 shows different experiments with a model Saturn cluster of a 1:100 scale. The exit Mach number is $M_{ex} = 2.4$. The jet is over-expanded; this means that the core length is smaller than that for an ideally expanded one. From configuration A, where only one engine was on, one can find x_c/d_o as approximately 9. The thrust of a single engine is given as $F = 9.63$ lbs. The expression $F/(\gamma_L n_o d_o^2)$ is formed by the parameters of one engine only. The penetration depth increases with increasing number of engines. This can be explained by a slight increase in core length and, above all, by less attenuation of the jet velocity of the combined engines, since the mixing process is delayed. However, if the engines are very far apart as in the case of configuration F, where the engines 2 and 4 are on, the jets act like single jets and consequently have the same penetration. Also an attempt was made to predict the penetration depth of the full scale booster with all eight engines on. It was found that the Saturn booster with the nozzle plane at sea level ($H/d_o = 0$) would have a penetration of approximately $n_o/d_o = 40$ to 48, which would correspond to about 170 to 205 feet. In Reference 10, a penetration depth of 169 feet was predicted without considering the compressibility. The minimum penetration, corresponding to $f = 1$, would be 170 feet.

IX. CONCLUSION

This investigation dealt with the penetration of a compressible gas jet into a liquid. To analyze and correlate test data, a simplified jet theory was used where the velocity decay follows a hyperbolic law. However, despite the simplifications, the theory correlates the available test data relatively well. Some uncertainty exists about the compressibility factor f of a jet. As long as the relative penetration is large, there need not be much concern about the factor f, since the Mach number on the centerline of the jet falls far down into the subsonic region.

The analysis shows also that for constant exit Mach number the jets of smaller thrust level have a larger dimensionless penetration depth than jets of large thrust level; scaling is therefore not possible, without changing the geometry of the rocket motor. However, with the help of the simplified theory, the prediction of the penetration depth is possible when the jet data are known.

18

Splash heights were found to be a function of the penetration depth n_o only after a critical value of n_o is surpassed. For large penetrations, the ratio s_c/n_o seems to be constant; however, more data must be gathered to confirm this statement.

For the penetration of rocket clusters, more parameters have to be considered and the possibility to predict the penetration with a certain accuracy decreases.

In principle, however, the same basic ideas which were applied to the single jet should apply also for a multitude of jets, as long as the important parameters are held constant. If this is done, one should be able to predict reasonably well the penetration depth of the prototype.
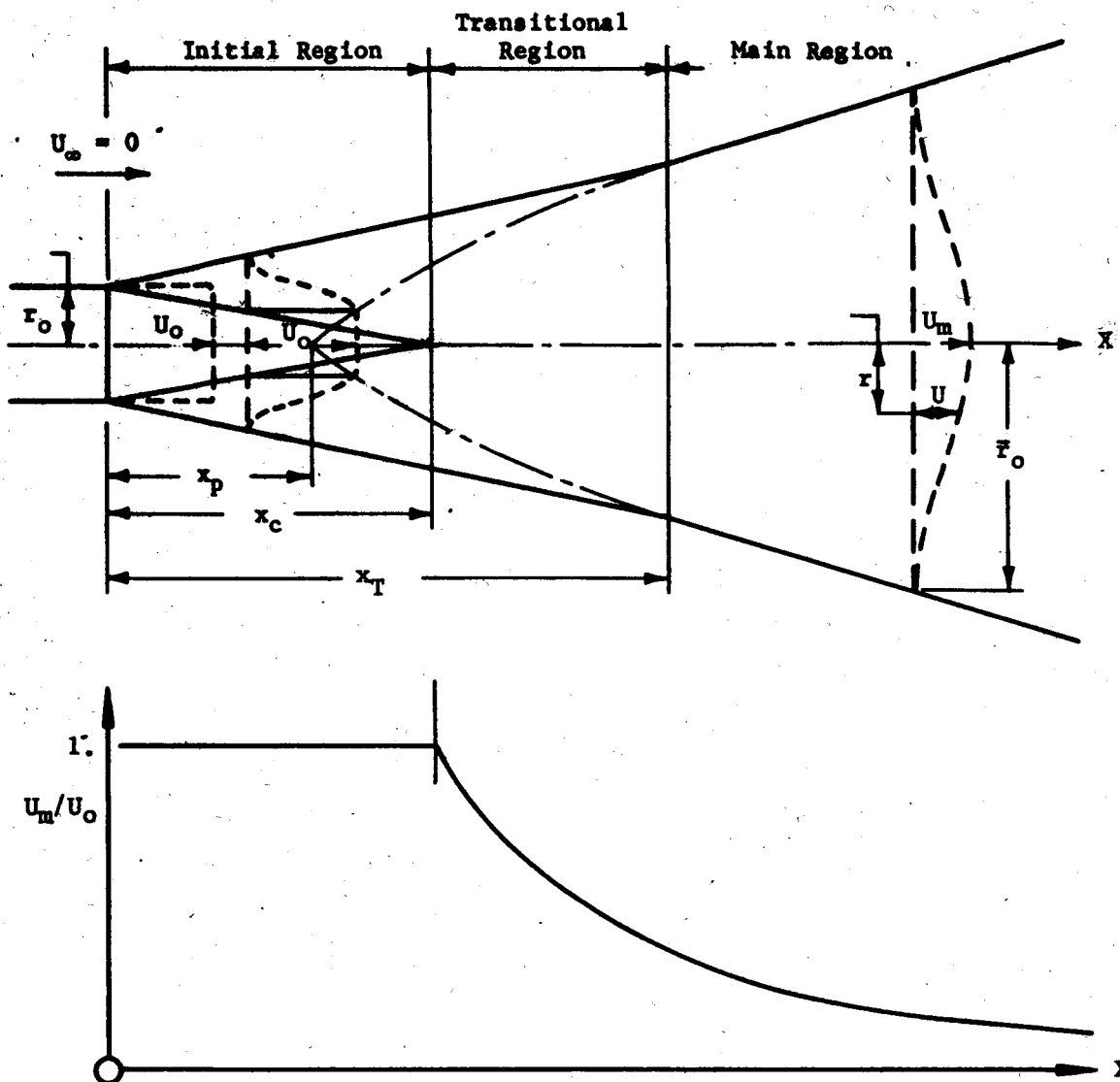
FIGURE 1. DIAGRAM OF A SUBMERGED JET AND VELOCITY DISTRIBUTION
ALONG THE AXIS OF THE JET
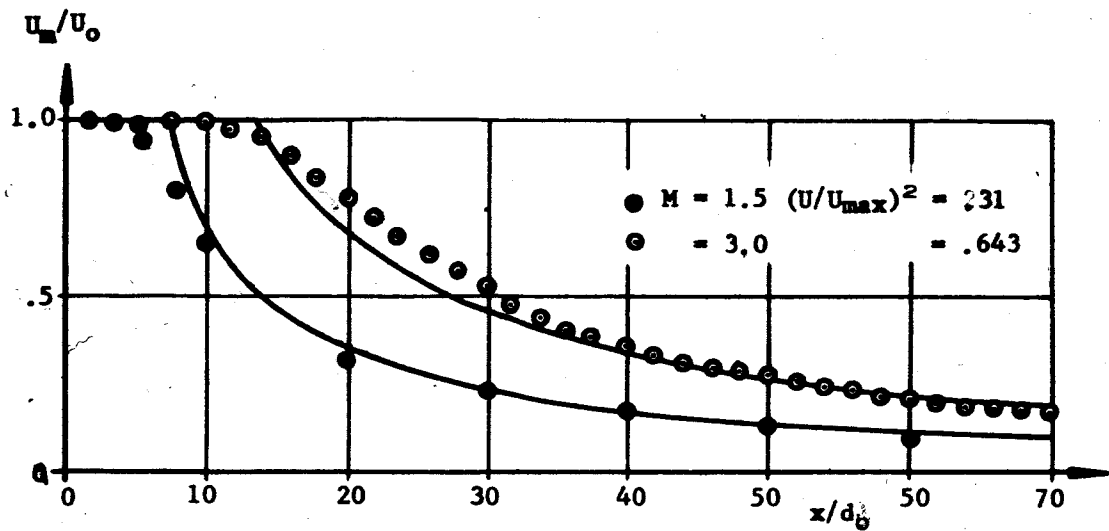
FIGURE 2. VELOCITY DISTRIBUTION ALONG THE CENTERLINE OF TWO SUPERSONIC JETS
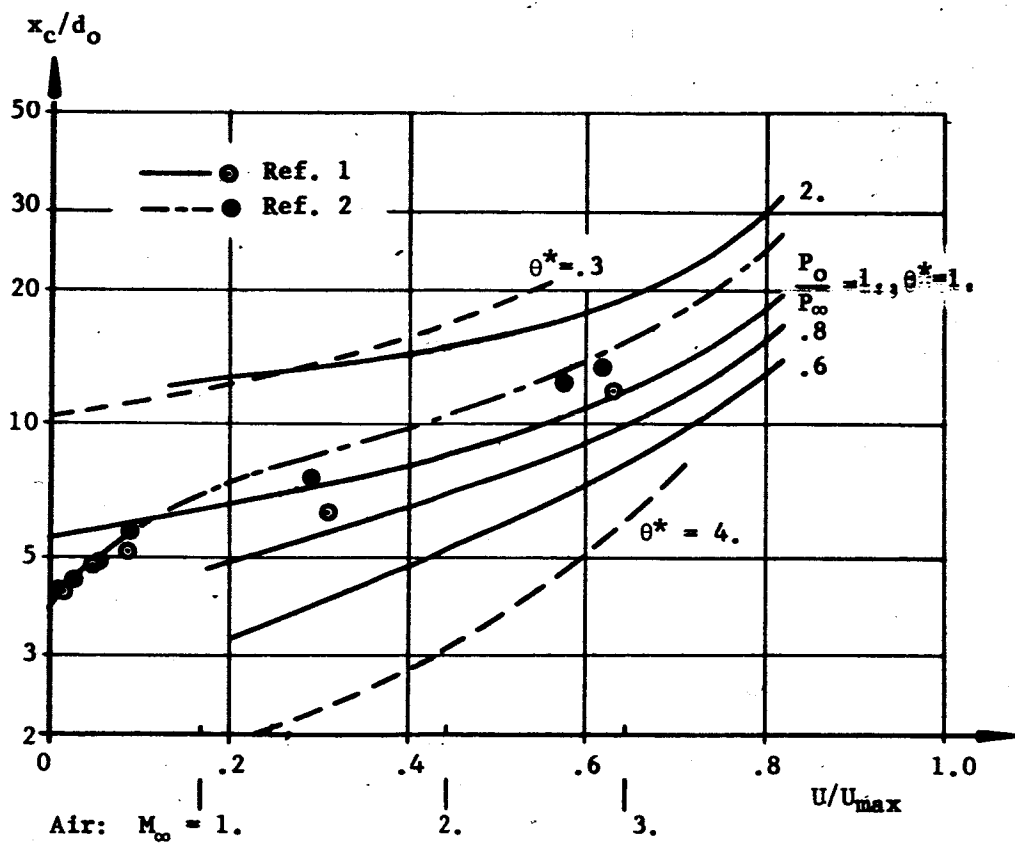
FIGURE 3. DIMENSIONLESS CORE LENGTH AS A FUNCTION OF THE MACH NUMBER WITH
TEMPERATURE AND EXPANSION RATIO AS PARAMETER
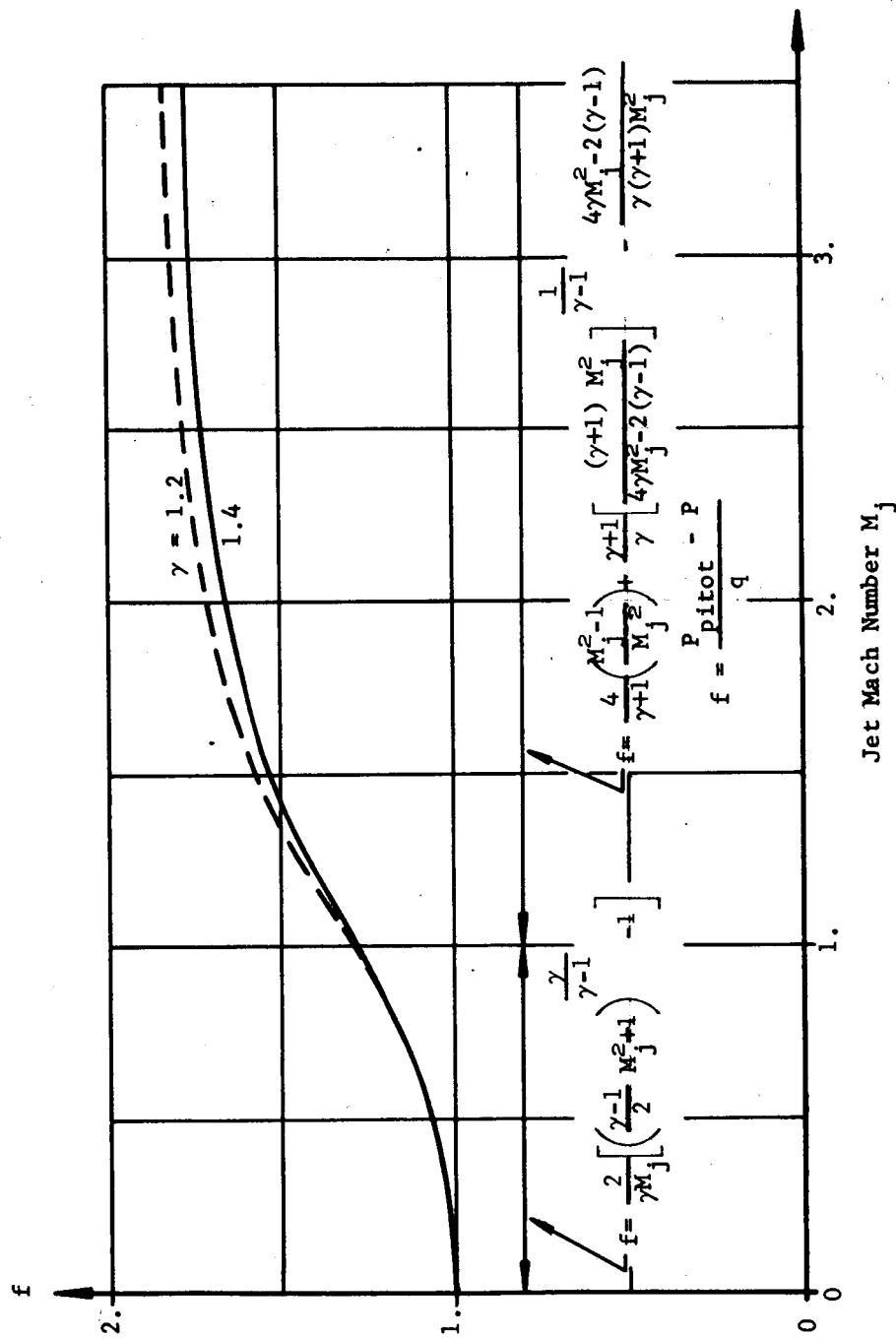
FIGURE 4. STAGNATION PRESSURE RATIO AS A FUNCTION OF THE MACH NUMBER IN FRONT OF THE NORMAL SHOCK
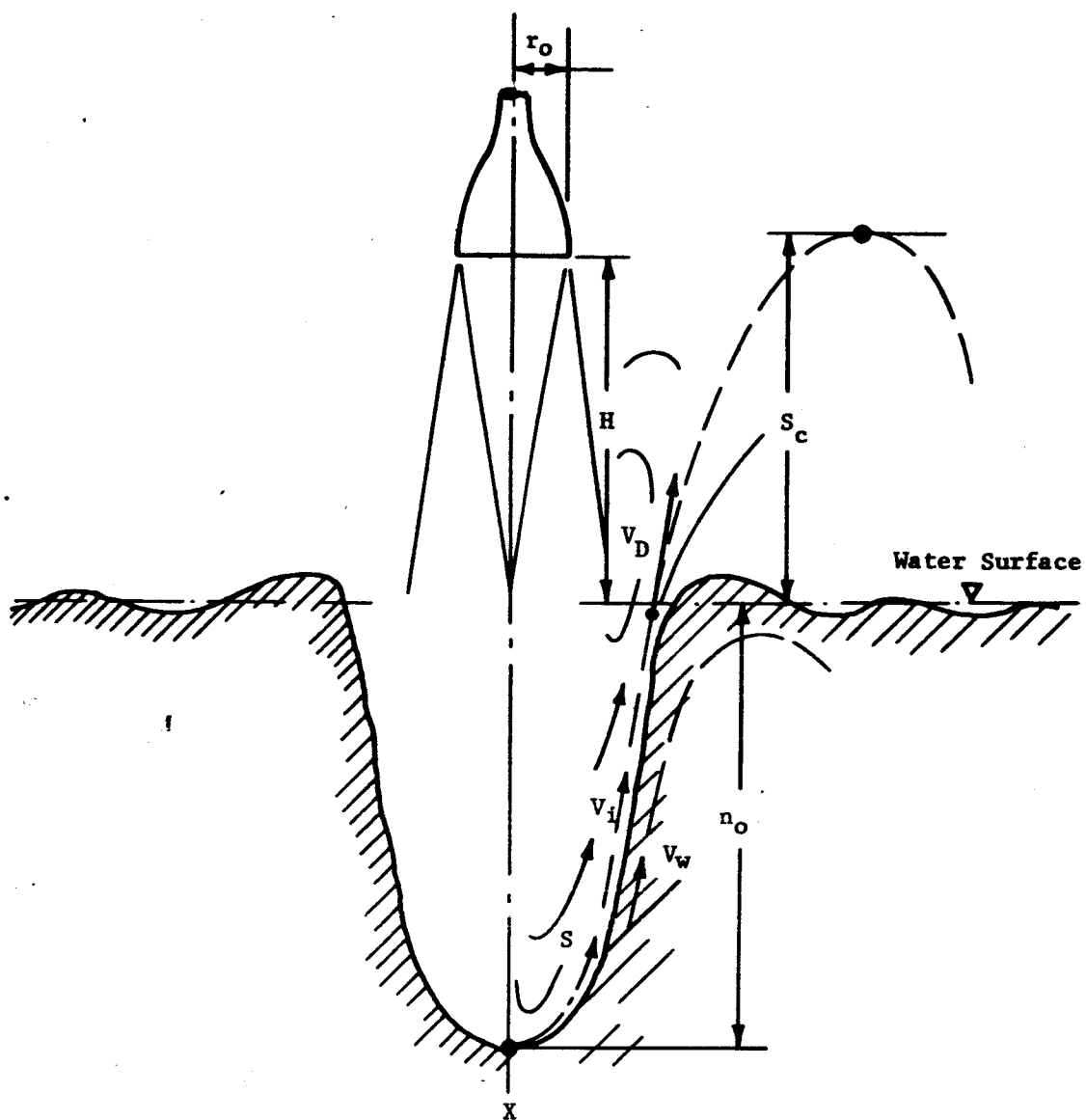
FIGURE 5. JET IMPINGING ON A LIQUID SURFACE
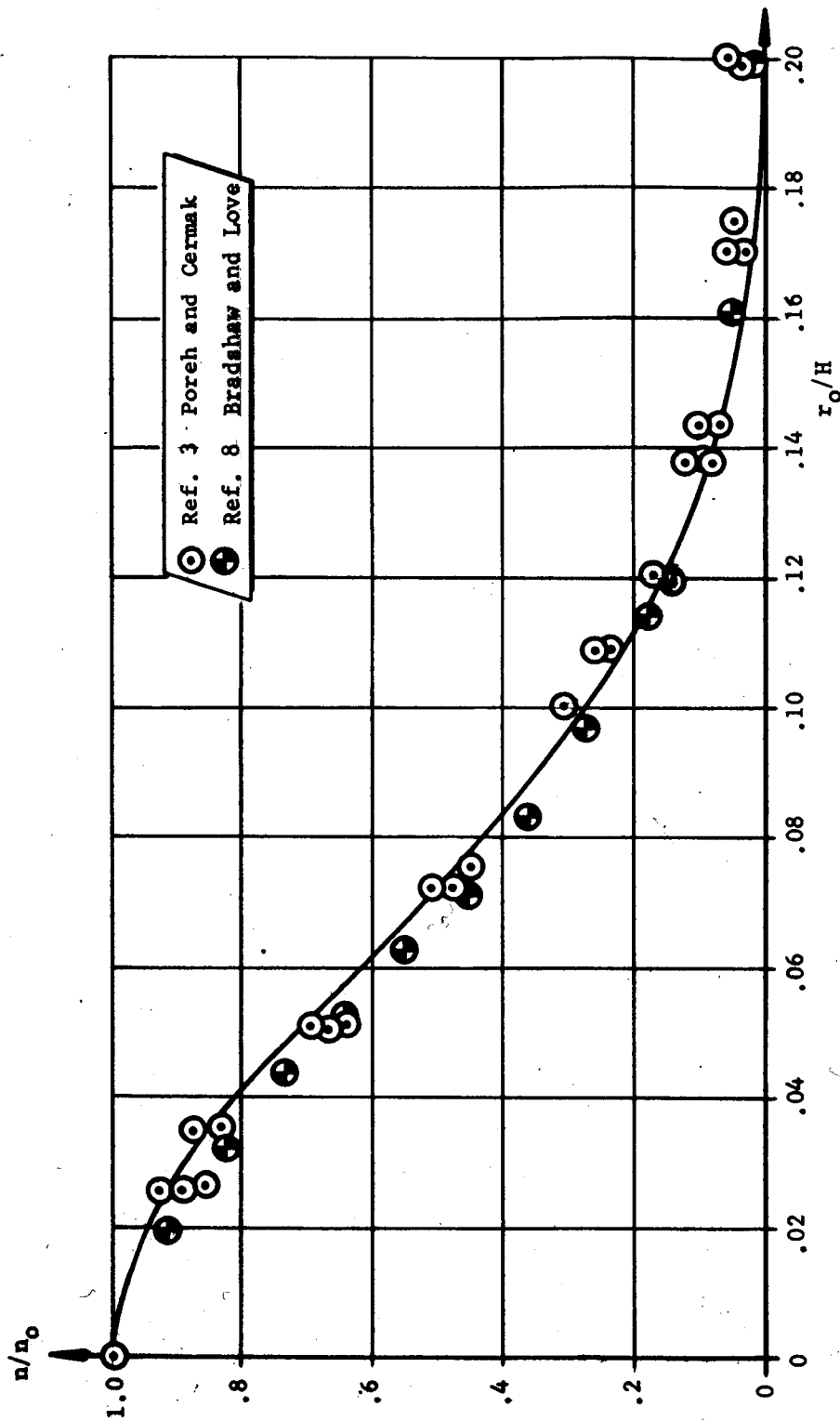
FIGURE 6. PRESSURE DISTRIBUTION OF A CIRCULAR TURBULENT JET IMPINGING ON A FLAT PLATE
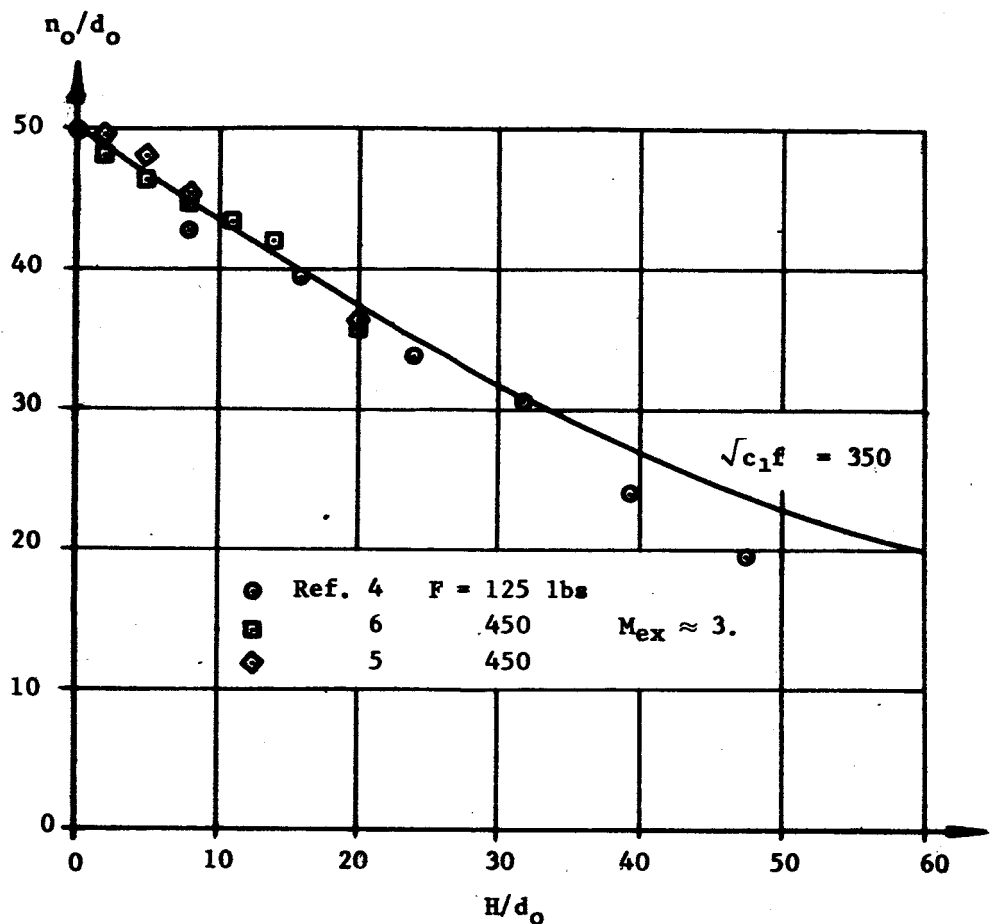
FIGURE 7. DIMENSIONLESS PENETRATION DEPTH AS A FUNCTION OF
STAND-OFF DISTANCE FOR SEVERAL JETS

Legend within Figure 7:

	Ref.		F = 125 lbs	
⊙	4	F =	125 lbs	
⊡	6		450	$M_{ex} \approx 3.$
◇	5		450	

Axis labels: n_o/d_o (vertical), H/d_o (horizontal), curve labeled $\sqrt{c_1 f} = 350$
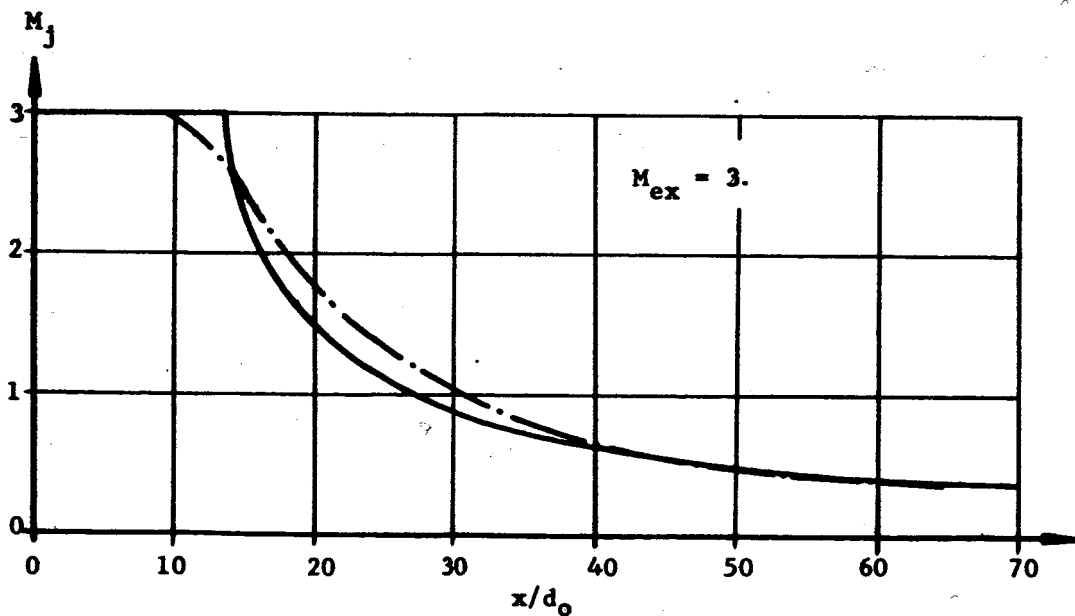
FIGURE 8. JET MACH NUMBER ALONG THE CENTERLINE OF THE JET

Axis labels: M_j (vertical), x/d_o (horizontal), $M_{ex} = 3.$
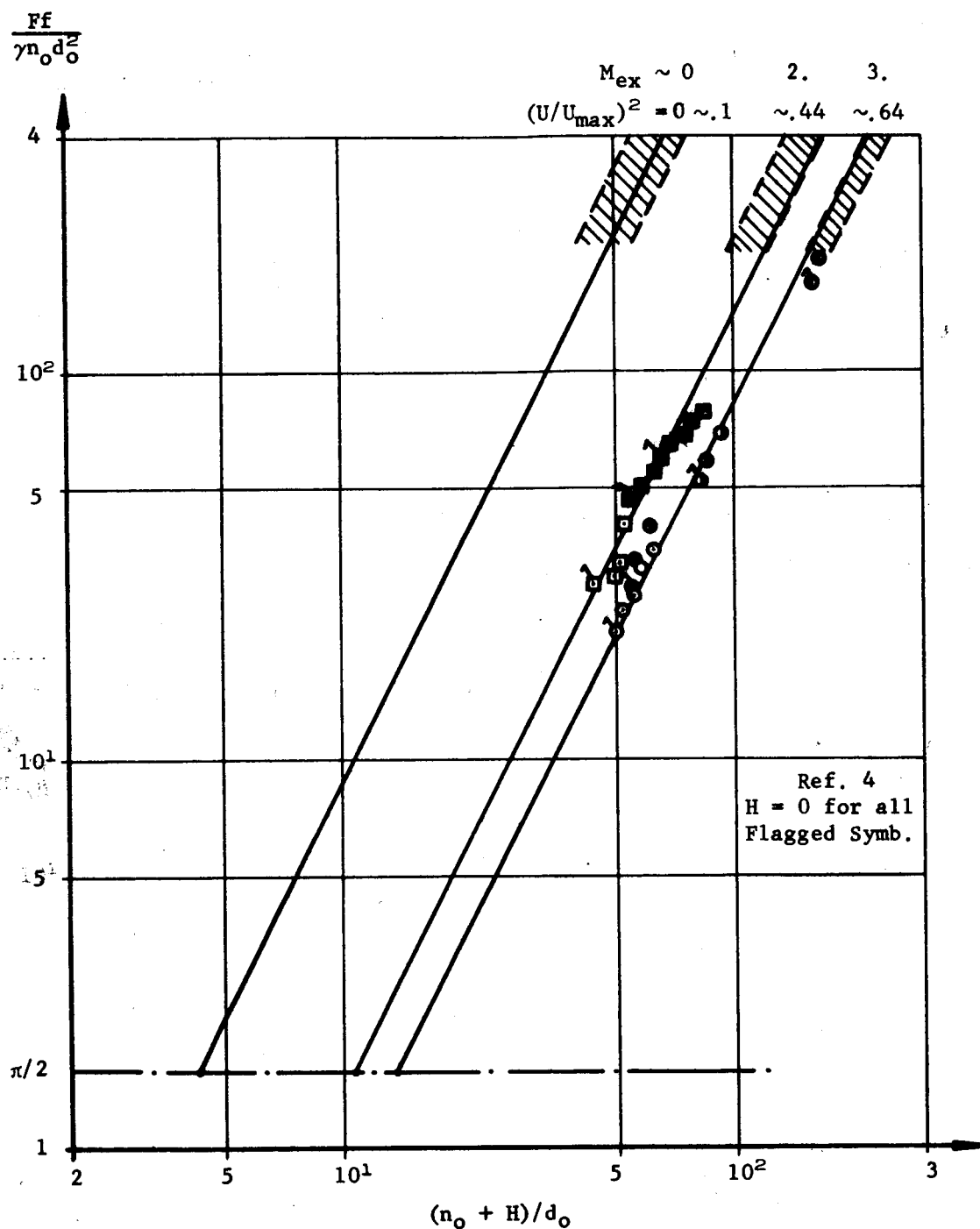
FIGURE 9.   CAVITY DEPTH FOR DIFFERENT MACH NUMBERS
(Air γ = 1.4, Chamber Temp. T_o = 90F.)
H/d_o from 0 to Approx. 30
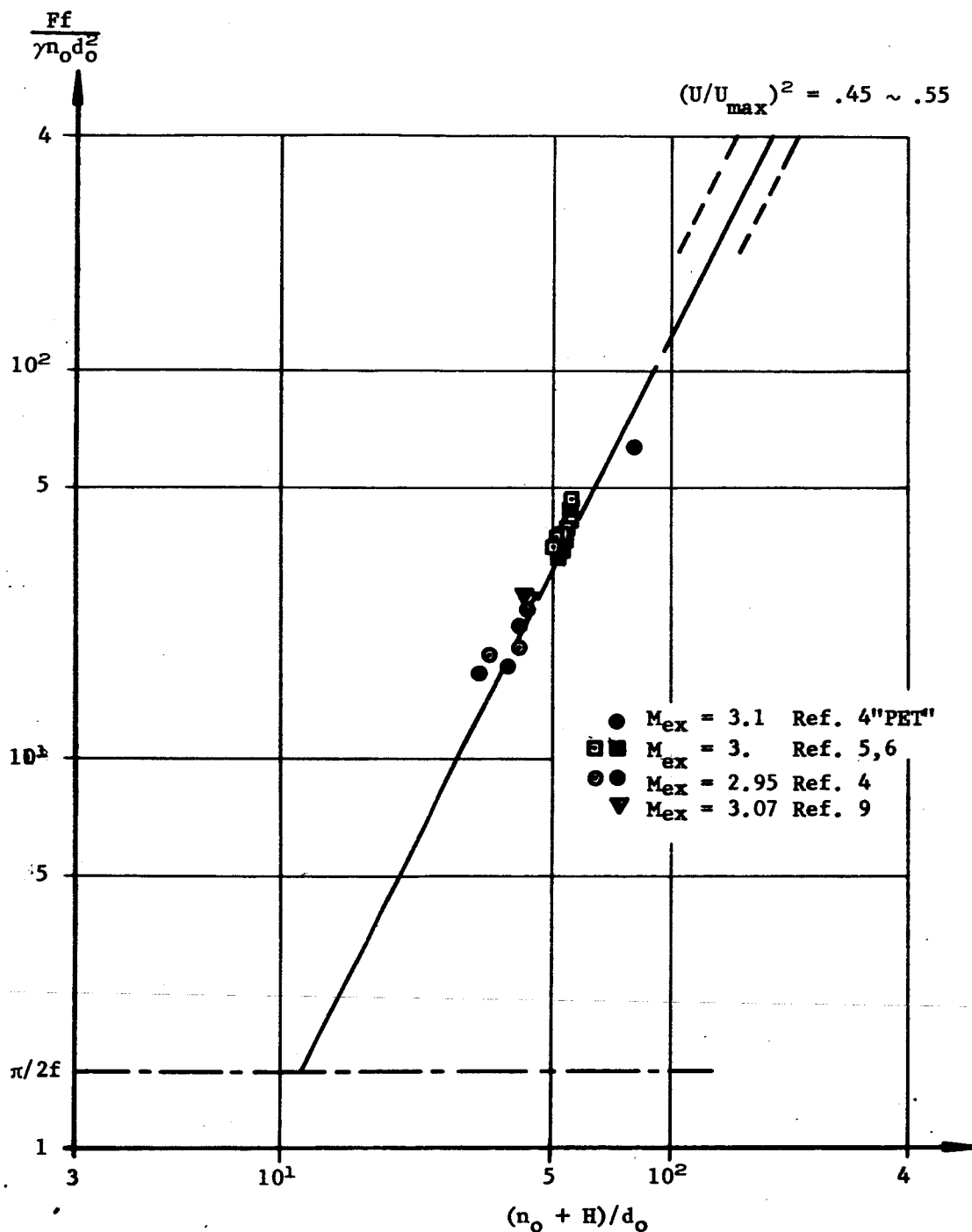
FIGURE 10. CAVITY DEPTH FOR ONE MACH NUMBER, H/d_o RANGING FROM 2 TO 30
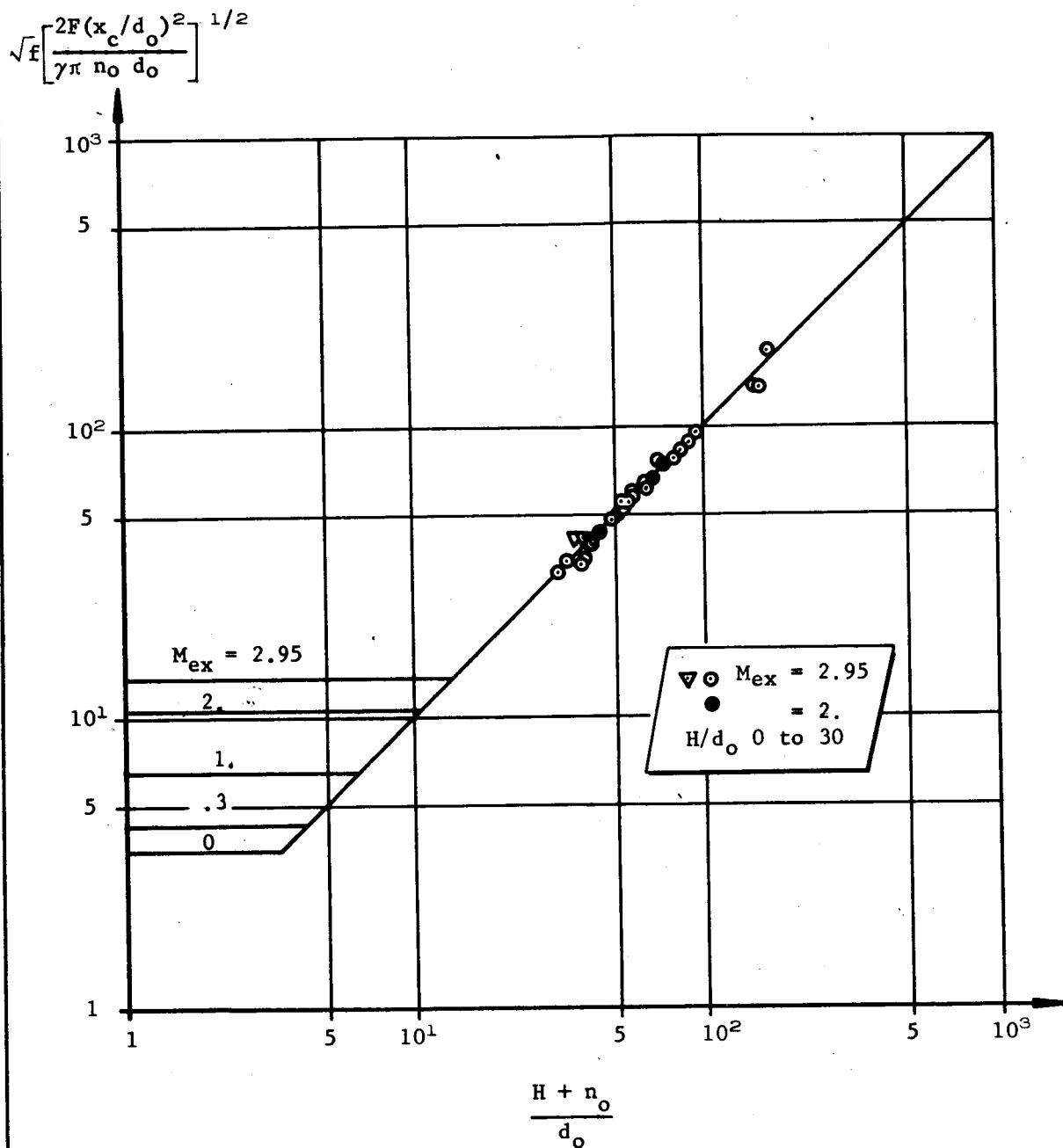
FIGURE 11. CORRELATION OF THE PENETRATION DEPTH FOR DIFFERENT SUPERSONIC JETS

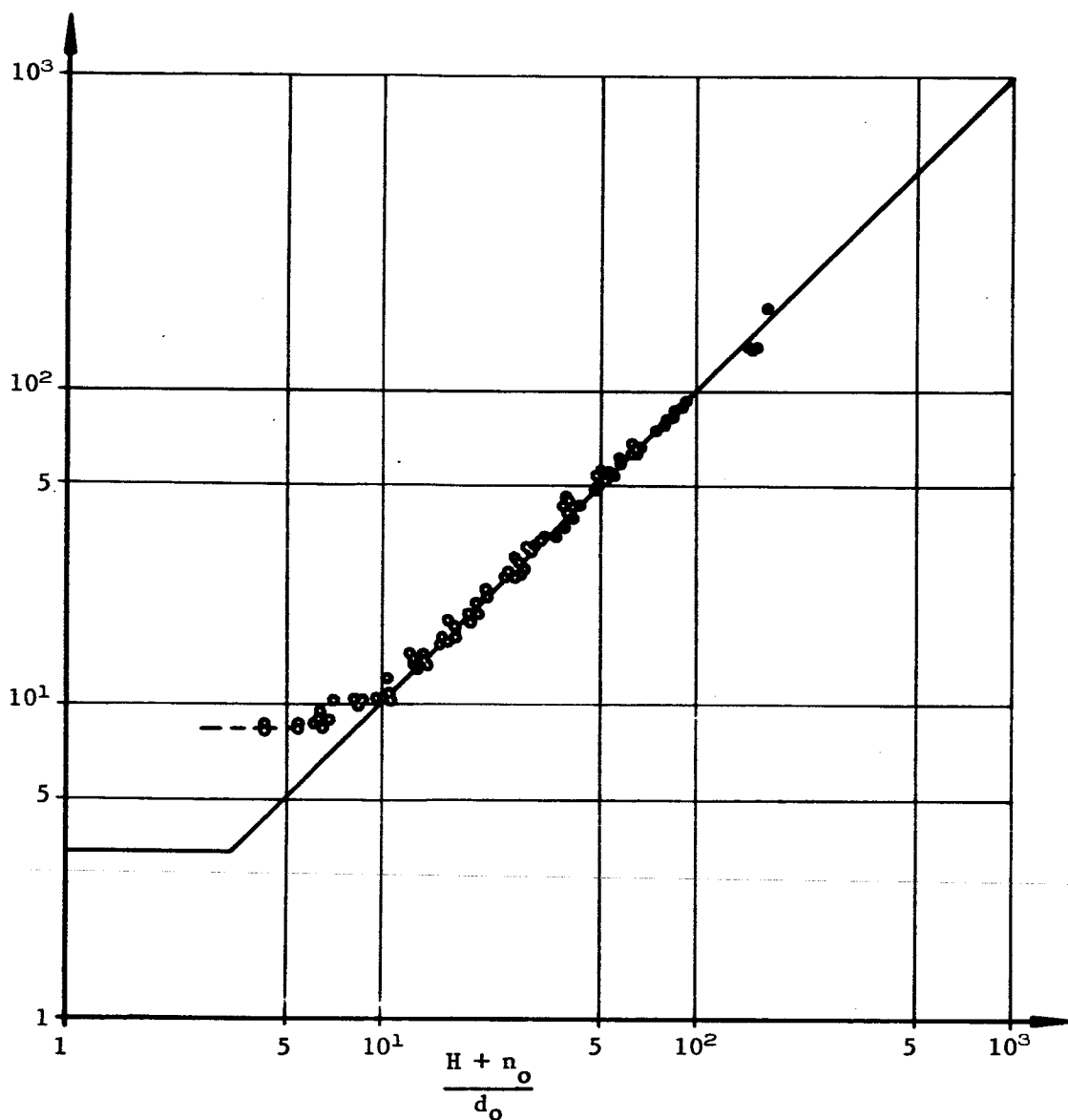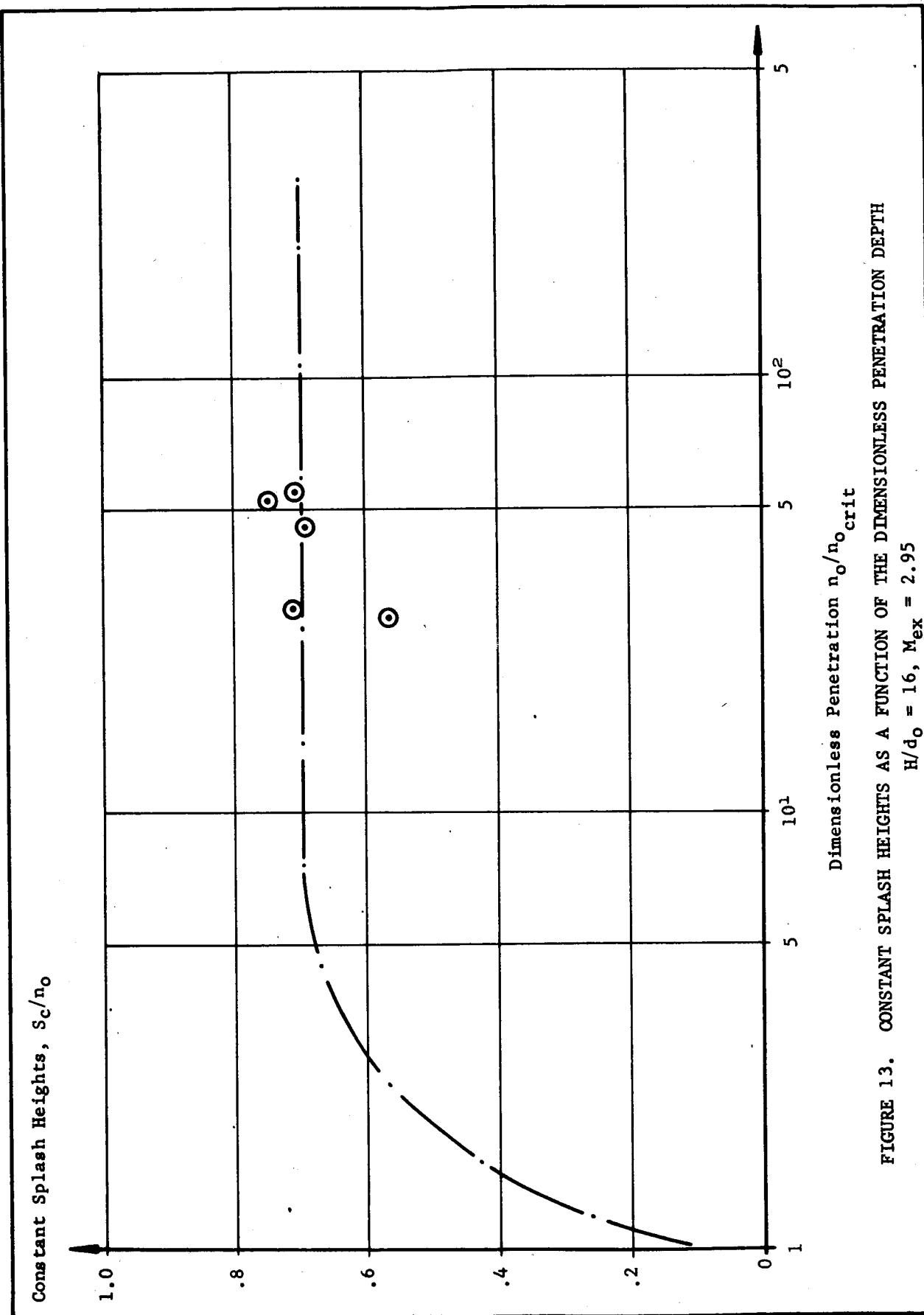$$\sqrt{f}\left[\frac{2F(x_c/d_o)^2}{\gamma\pi\ n_o\ d_o^2}\right]^{1/2}$$

FIGURE 12. CORRELATION OF THE PENETRATION DEPTH FOR
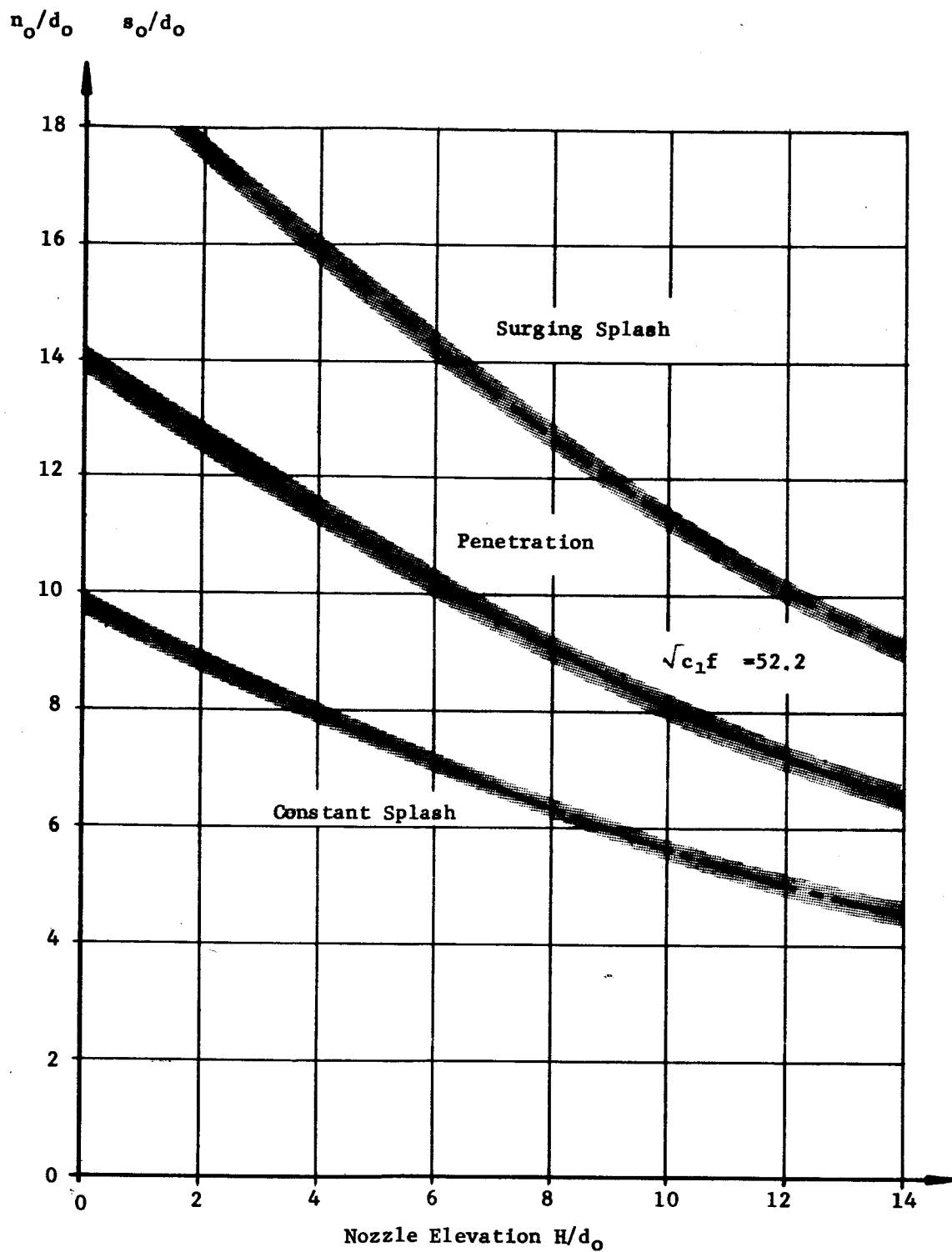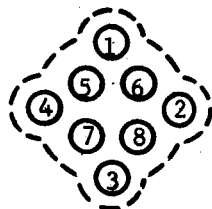DIFFERENT SUBSONIC AND SUPERSONIC JETS

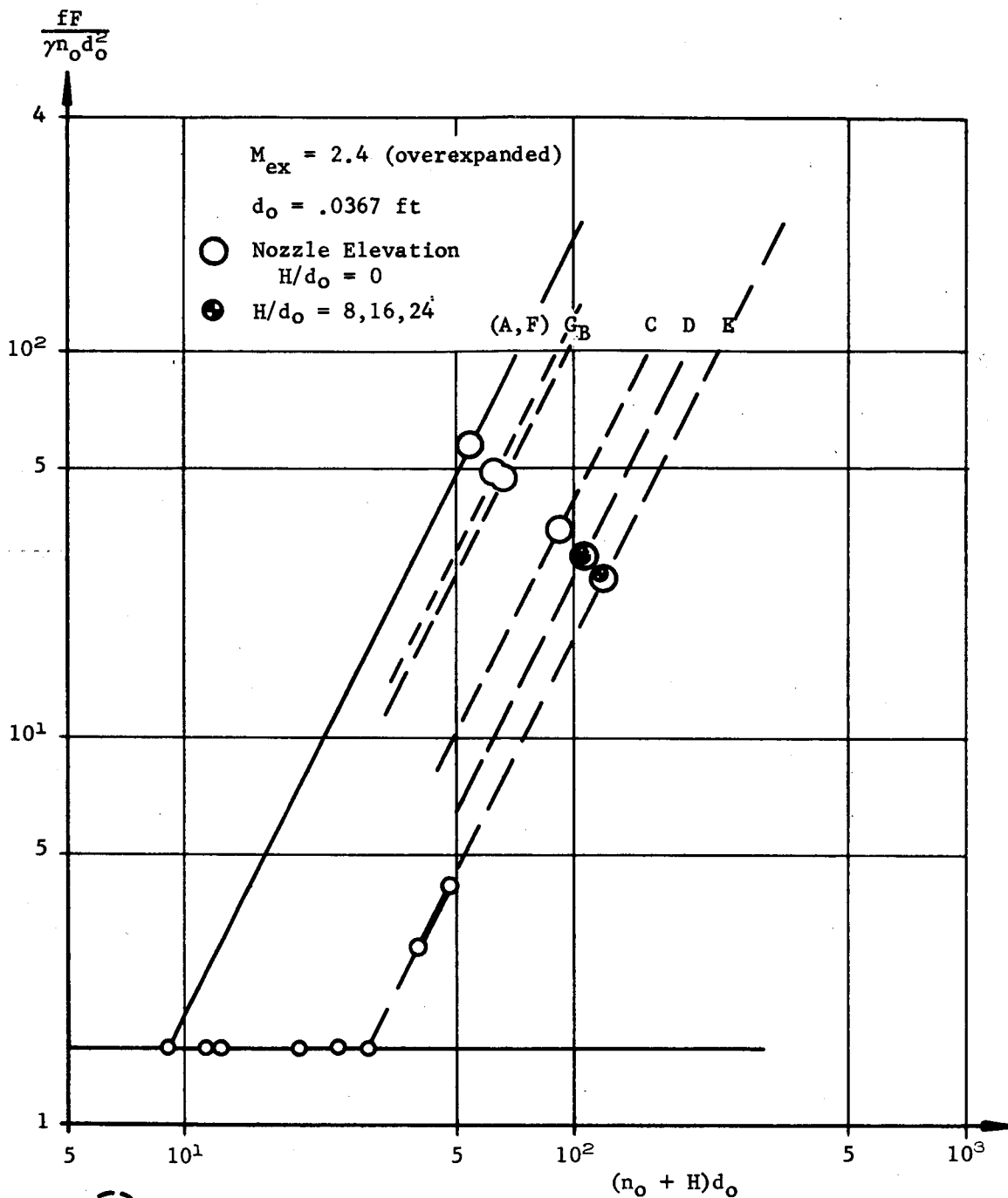FIGURE 13. CONSTANT SPLASH HEIGHTS AS A FUNCTION OF THE DIMENSIONLESS PENETRATION DEPTH

$H/d_o = 16$, $M_{ex} = 2.95$

FIGURE 14. JET PENETRATION AND SPLASH HEIGHTS FOR ONE F-1 ENGINE

FIGURE 15. PENETRATION DEPTH FOR A MODEL-SATURN CLUSTER
WITH DIFFERENT ENGINES ON

REFERENCES

1. Abramovich, "The Theory of Turbulent Jets," (Translation, the M.I.T. Press).

2. "Suppression of Jet Noise with Emphasis on the Near Field Flight Dynamics Lab.," Wright Patterson AFB, Ohio, ASD-TDR-62-578.

3. Banks, Robert and D. V. Chandrasekhara, "Experimental Investigation of the Penetration of a High Velocity Gas Jet Through a Liquid Surface," Journal of Fluid Mechanics 15.

4. Anderson, C. A., J. H. Hubbart, and E. A. Lotz, "Exhaust Blast Effect Studies for Large Super Boosters," Technical Report No. 1-21-ORDL-U. S. Army Engineer Division, Ohio, January 1962.

5. Harsh, M. G., Jr., "Jet Impingement Test-Turbine Report - Tests C-002-17 through C-002-45," Feb. 27, 1964, R-TEST-CTE.

6. Perry, Guy D., "Jet Impingement Test - Interim Report Tests C-002-12a, b, 13a, 14, 15 and 16," October 23, 1963, R-TEST-CT.

7. Collins, R. D. and H. Lubansk, "The Depression of Liquid Surfaces by Gas Jets," British Iron and Steel Research Association, London, W. I., Brit. Journal of Appl. Physics, Vol. 5, Jan. 54.

8. Bradshaw, P. and E. M. Love, "The Normal Impingement of a Circular Air Jet on a Flat Surface," N.P.L. R M No. 3205, 1961.

9. Harsh, G., "Transmittal of Jet Impingement Test Data, Tests G-002-59 through G-002-76," R-TEST-CT No. 82-64, June 5, 1964.

10. Anderson, C. A., J. H. Hubbard, and E. A. Lotz, "Jet Blast Attenuation for Large Super Booster," AS Army Engineer Division, Ohio Technical Report No. 1-16, January 1961.

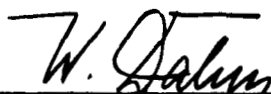11. Lamb, H., Hydrodynamics, Dover Publications, Sixth Edition, 1932.

JET PENETRATION INTO A LIQUID

By

H. G. Struck

The information in this report has been reviewed for security classification. Review of any information concerning Department of Defense or Atomic Energy Commission programs has been made by the MSFC Security Classification Officer. This report, in its entirety, has been determined to be unclassified.

This document has also been reviewed and approved for technical accuracy.

_____

Werner K. Dahm
Chief, Aerodynamics Division

_____

E. D. Geissler
Director, Aero-Astrodynamics Laboratory

34

DISTRIBUTION

DEP-T

HME-P

CC-P

MS-T
  Roy Bland

MS-H

MS-IP

MS-IPL

K-D
  Mr. Popell
  Mr. vonTiesenhausen
  Mr. Valentine (20)
  Mr. Davis

R-TEST
  Mr. Heimburg
  Mr. Grafton
  Mr. Verschoore
  Mr. Perry
  Mr. Williams
  Mr. Countess (6)

R-AERO
  Dr. Geissler
  Mr. Dahm
  Mr. Holderer
  Mr. Warmbrod
  Mr. Sims
  Mr. Struck (10)

Technical & Scientific Information Facility (25)
P. O. Box 5700
Bethesda, Md.
Attn: NASA Rep. (S-AK/RKT)